Journal of Zhejiang University-SCIENCE A (Applied Physics & Engineering) 2024 25(1):79-96
www.jzus.zju.edu.cn; www.springer.com/journal/11582
E-mail: jzus_a@zju.edu.cn

Research Article

https://doi.org/10.1631/jzus.A23D0045

Biomimetic microchannel network with functional endothelium formed by sacrificial electrospun fibers inside 3D gelatin methacryloyl (GelMA) hydrogel models

Haoyu SUN, Haiyang MA, Li WANG, Yang LIU, Tian HOU, Wenjie TANG, Qing YU, Meiwen AN✉, Meiling WEN✉

Institute of Biomedical Engineering, College of Biomedical Engineering, Taiyuan University of Technology, Taiyuan 030024, China

Abstract: Three-dimensional (3D) hydrogel models play a crucial role in tissue engineering for promoting tissue regeneration. A biomimetic microchannel network system in the 3D hydrogel model is necessary for optimal cellular function. This report describes the preparation of a biomimetic hydrogel scaffold with an internal microchannel network, using electrospinning techniques and the sacrificial template method for 3D cell culture. Microchannels and cavities were created within the gelatin methacryloyl (GelMA) hydrogel by sacrificing polyvinyl alcohol (PVA) electrospun fibers (>10 μm), resulting in the creation of microvessel-like channels. Mechanical characterizations, swelling properties, and biodegradation analysis were conducted to investigate the feasibility of a biomimetic microchannel network hydrogel scaffold for 3D cell culture applications. Compared to pure GelMA hydrogel, the hydrogel with microchannels promoted cell proliferation, adhesion, and endothelial tube formation. Moreover, the results confirmed that the biomimetic microchannel network scaffold had a major impact on the distribution and arrangement of human umbilical vein endothelial cells (HUVECs) and can enable the formation of artificial microvasculature by the culture of HUVECs and cell media perfusion.

Key words: Biomimetic scaffold; Photocrosslinking; Microchannel network; Tissue engineering; Artificial microvascular

1 Introduction

Although traditional two-dimensional (2D) cell cultures have been used as in vitro models to study cell behavior from biophysical and biochemical cues, the 2D systems can result in cell bioactivities that, under some circumstances, deviate appreciably in their in vivo response. Cell–cell and cell–matrix interactions in 3D hydrogel models are more comparable to in vivo conditions (Duval et al., 2017; Roh et al., 2019; Türker et al., 2019; Lovett et al., 2020). Moreover, the tissue scaffolds that closely mimic native tissues require specific extracellular matrix (ECM) composition and complex material structures, which can achieve diffusion of oxygen and nutrients and exchange of waste in larger biological scaffolds (Rnjak-Kovacina et al., 2014). Therefore, the fabrication of 3D artificial scaffold models that can mimic native tissues in structure and properties and with microvascular systems remains a major challenge (Rouwkema et al., 2008; Rademakers et al., 2019; Xia and Luo, 2022).

Fully developed vascular networks of 10 μm in diameter are essential for cell growth and tissue formation (Buchwald, 2009; Zohar et al., 2018; Zia et al., 2022). Therefore, it is necessary to form perfusable microchannel networks to ensure the survival of larger artificial tissues (Ryma et al., 2022). Furthermore, cut-off distances of more than 200 μm between cells and the vascular system have been reported as resulting in a significant reduction in cell viability. An upper limit of (232±22) μm has been experimentally observed for oxygen diffusion distances based on a 3D sphere in vitro measurement (Groebe and Mueller-Klieser, 1991; Chang and Niklason, 2017). At present, existing microvascular networks within artificial 3D tissue models are larger than 100 μm in diameter. Therefore,

✉ Meiwen AN, anmeiwen@tyut.edu.cn
Meiling WEN, wenmeiling@tyut.edu.cn
Meiling WEN, https://orcid.org/0009-0004-5918-3099

Received Apr. 12, 2023; Revision accepted Apr. 28, 2023;
Crosschecked Dec. 13, 2023

it is important to develop tighter patterning of the microchannel network to mimic the complexity of native tissues (Moulisová et al., 2017; Enrico et al., 2022).

In recent years, advances in manufacturing technology have made the creation of complex 3D vascular systems possible. In particular, 3D bioprinting-based methods, such as inkjet printing (Therriault et al., 2003; Zhao et al., 2022), extrusion printing (Hinton et al., 2015; Shiwarski et al., 2021), and stereolithography printing (Mota et al., 2015), allow the generation of in situ microchannels in 3D hydrogel structures containing cells. However, these techniques lead to reduced cell viability. More importantly, limitations by resolution make it difficult to prepare microvascular networks (Cicha et al., 2017; Liaw and Guvendiren, 2017; Dogan et al., 2020; Kumar and Sharma, 2021). Electrospinning (Wittmer et al., 2011; Kim and Kim, 2014; Kurakula and Koteswara Rao, 2020; Toriello et al., 2020) is one of the most established and advanced fabrication techniques, producing fibres from the nano- to micron-scale that resemble the fibrous and porous structure of natural ECM and the network-like structure of microvessels (Boakye et al., 2015; Edwards et al., 2015; Wan et al., 2018; Bacakova et al., 2019; Li et al., 2021). Such interconnected porous fibres provide easy transport of nutrients and removal of metabolic waste, which is important for cell growth and tissue regeneration (Türker et al., 2019).

An artificial 3D matrix should mimic the complex cellular microenvironment with a unique combination of biological and physical properties, including biocompatibility as they mimic ECM, tunable mechanical, swelling, and degradation properties that promote cell survival, behavior, and response in the 3D environment (Uppuluri et al., 2022; Xu et al., 2022). Amongst natural hydrogels, collagen is one of the most commonly used biomaterials as it is the main component of the ECM in tissues to support cell proliferation, migration, and differentiation (Helary et al., 2011). However, collagen hydrogels have some limitations such as low mechanical properties and rapid degradation rates (Helary et al., 2010). Additionally, there is potential toxicity caused by chemical cross-linking agents (e.g., glutaraldehyde) of collagen, which are commonly used to improve the mechanical properties and stability of hydrogels (Hu et al., 2010; Chamorro et al., 2016). Gelatin methacrylate (GelMA), the hydrolysis product of collagen, contains Arg-Gly-Asp (RGD) sequences that promote cell attachment, as well as matrix metalloproteinase (MMP) target sequences suitable for cell remodeling (Nichol et al., 2010; Bae et al., 2011; Zhao et al., 2016; Xiao et al., 2019; Bupphathong et al., 2022). The advantages of GelMA over collagen are its better solubility and lower immunogenicity (van den Bulcke et al., 2000). This polymerization can occur under mild conditions (room temperature, neutral pH, aqueous environment, etc.) and allows for temporal and spatial control of the reaction (Nichol et al., 2010; Bae et al., 2011). This allows the creation of unique patterns, morphologies, and 3D structures in microprocessed hydrogels, providing an ideal platform, including the formation of microvascular networks, for controlling cell behavior, cellular biomaterial interactions, and tissue engineering (Aubin et al., 2010; Nichol et al., 2010; Chen et al., 2012; Lin et al., 2013; Bertassoni et al., 2014; Pien et al., 2021).

As research on 3D tissue engineering scaffold progresses, molecules and cells in networks can be made to diffuse through the interconnected pores and microchannels by the combination of electrospinning and 3D bioprinted structures (Li et al., 2021; Wang et al., 2022). However, researchers have mostly limited themselves to the use of nanofibres as bionic in vivo ECM structures to provide 3D structures (Kenar et al., 2019; Nazarnezhad et al., 2020). Therefore, we developed novel 3D microchannel network biomimetic hydrogel scaffolds combined with GelMA hydrogels and sacrificial electrospun fibers (>10 μm) using electrospinning technology (Scheme 1). The physical properties of the hydrogels were modulated by systematically varying the GelMA concentration to control their mechanical properties, degradability, swelling, and the feasibility of forming microchannels within the hydrogels. Human umbilical vein endothelial cells (HUVECs) were used as a model to study cell biocompatibility, cell adhesion, and proliferation in 3D GelMA hydrogel scaffolds. Overall, this paper presents novel biomimetic hydrogel scaffolds containing a microchannel network system to promote the distribution and alignment of endothelial cells for generating vascularized tissue models.

2 Experimental

2.1 Materials

Polyvinyl alcohol (PVA, analytical reagent, number-average polymerization degree of 98.0%–99.0%) was

purchased from Aladdin Chemistry Co., Ltd. (Shanghai, China). Hexafluoroisopropanol (HFIP), gelatin (from porcine skin, Type A, 300 bloom), and methacrylic anhydride (MA) were obtained from Macklin Chemistry Co., Ltd. (Shanghai, China). Lithium phenyl-2,4,6-trimethyl-benzoylphosphinate (LAP) was acquired from Shanghai Yuanye Bio-Technology Co., Ltd. (Shanghai, China). Phosphate-buffered saline (PBS, pH 7.4 10×, Gibco), High Glucose Dulbecco's Modified Eagle's Medium (DMEM), Fetal Bovine Serum (FBS), and Cell Counting Kit-8 (CCK-8) were purchased from Pulilai Gene Technology Co., Ltd., China. The LIVE/DEAD Viability/Cytotoxicity Kit was obtained from Beyotime Biotechnology Co., Ltd., and 4'6-diamidino-2-phenylindole (DAPI) and F-actin were procured from Solarbio Co., Ltd. (Beijing, China).

2.2 Materials fabrication of sacrificial template fibers

As a sacrificial material for generating the channel network, PVA solutions of different proportions were prepared by dissolving 10% or 15% (mass fraction) PVA in different ratios of deionized water and HFIP and stirring for 12 h. The PVA solution was electrospun through a 5 mL syringe and an 18G needle. The high-voltage power supply was 5 kV or 10 kV, the push rate was 10 mL/h, the distance between the needle and the drum receiver was 10–20 cm, and the drum receiver speed was 20 r/min to spin a more uniform micron fibre structure. The collected sacrificial micron fibres were placed in a vacuum drying oven and freeze dried for 48 h prior to the next characterisation step and cell studies.

2.3 Characterisation of sacrificial template fibers

The morphological structure of PVA electrospun micron fibers was observed using scanning electron microscopy (SEM) to characterize the surface morphology of the fibers after gold spraying of the film. ImageJ was used to measure the average diameter of the PVA fibers in at least 50 randomly selected positions.

To analyze the degradability of the fibers in PBS solution, the electrospun membranes were cut into squares of approximately 30 mg and incubated in PBS solution at 37 °C. Three parallel samples of each sample were taken. The fibers were dried in a vacuum desiccator and weighed at predetermined time points (1 min, 3 min, 5 min, 10 min, 15 min, 20 min, 30 min, and 60 min). The initial weight was recorded as m_0, and the weight at the time points was recorded as m_1. The rate of fiber dissolution was determined by calculating the weight-loss. The degradation rate of the fibers (D) was determined by

$$D = \frac{m_0 - m_1}{m_0} \times 100\%. \tag{1}$$

2.4 Synthesis of GelMA

Briefly, Type A pig skin gelatin (10.0 g) was added to 100 mL of PBS to prepare a gelatin solution at a concentration of 0.1 g/mL. Then 0.5 mL of MA was added dropwise to the gelatin solution at a rate of 0.5 mL/min and stirred vigorously at 50 °C to react with the gelatin. Then, after 2 h, the reaction was terminated by adding 400 mL of PBS solution. The solution was

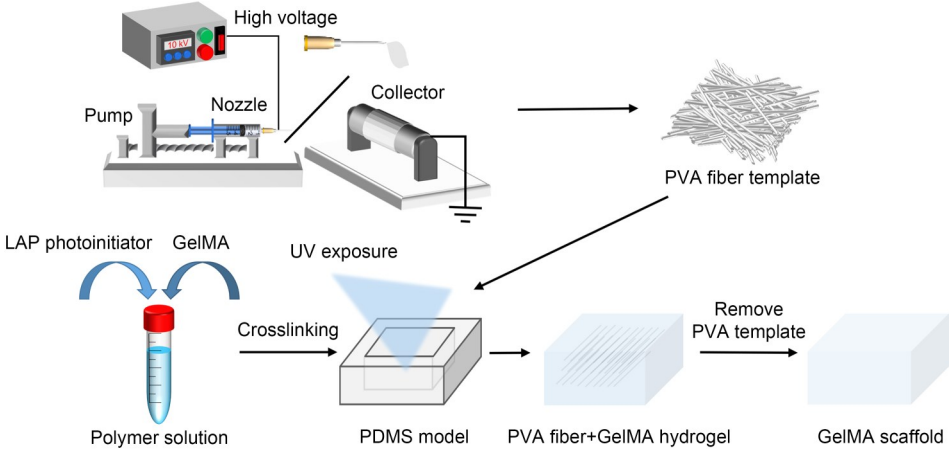

Scheme 1 Schematic diagram of the fabrication of a microchannel GelMA biomimetic hydrogel scaffold by sacrificial electrospinning of fibers, including the electrospinning process and the sacrificial removal of PVA fibers within the GelMA hydrogel. PDMS: polydimethylsiloxane. UV: ultraviolet

centrifuged at 3500 r/min for 10 min to remove precipitated impurities and poured into a 12–14 kDa dialysis bag of deionized water at 40 ℃ for one week to remove methacrylic acid by-products and unreacted MA. The product was then lyophilized and stored at −20 ℃.

Fourier-transform infrared spectra (FTIR) of GelMA were measured to determine if the synthesis was successful. Gelatin, GelMA, and GelMA hydrogel were freeze-dried, crushed in a pestle and mortar, and mixed with potassium bromide (KBr) powder in a ratio of 1:100 (in mass) and poured into a mold to be pressed into a transparent sheet. Data were collected by Fourier infrared spectrometer.

High-resolution proton nuclear magnetic resonance hydrogen spectroscopy (^{1}H-NMR) of GelMA was used to determine the degree of substitution of the synthesized GelMA. Before measurement, 50 mg of gelatin and GelMA were dissolved in 1 mL of deuterium oxide (D_2O), separately. A baseline correction was applied before obtaining the peak region of interest. The degree of methacrylamide modification was determined by

$$D_s = \frac{N_1}{N} \times 100\%, \tag{2}$$

where N_1 is the number of methacrylate groups, and N is the number of amine groups on unreacted polymers.

2.5 Micromorphology of GelMA hydrogels

The photoinitiator LAP was heated in a water bath at 40–50 ℃ and dissolved in PBS for the preparation of a pre-crosslinking solution of GelMA. The synthesized GelMA was irradiated with the above photoinitiator LAP for 15–30 s and placed in a refrigerator at −20 ℃ for 20 h. The GelMA hydrogels were then freeze-dried at −80 ℃. Before being sprayed with gold and observed by SEM, the GelMA hydrogels were placed in an ultra-low temperature refrigerator at −80 ℃ overnight and vacuum freeze-dried for 12 h. Porosity was quantified from SEM images by ImageJ software to determine pore size; six pictures for each condition were used for the purpose.

2.6 Fabrication of channel network hydrogels

The GelMA pre-crosslinking solutions were prepared at concentrations of 15%, 20%, and 25% (mass fraction, noted as G-15, G-20, and G-25). The prepared pre-crosslinking solution and the sacrificial fiber material were simultaneously added to a polydimethylsiloxane (PDMS) mold and then quickly irradiated with a 405 nm UV light source for gel crosslinking. Because of the low alcoholysis degree, PVA has a temperature-dependent water solubility, which decreases as the temperature gradually increases. After the temperature was reduced to room temperature, the fibers were dissolved by immersion for 1–2 h and eluted by squeeze infusion water washing. In this way, a network of void channels was created after the fibers had been dissolved and washed by infusion. The channel network scaffolds formed inside the above-mentioned hydrogels at different concentrations are noted as GC-15, GC-20, and GC-25.

2.7 Mechanical properties measurement

The compressive mechanical properties of the hydrogels were determined by a universal testing machine (INSTRON 5544, USA) using a 50 N pressure transducer. Compressive stress tests were performed on different concentrations of pure GelMA hydrogels and channel network hydrogel scaffolds. For the compression tests, test samples were prepared in a cylindrical shape (10 mm diameter and 2 mm thickness). The samples were incubated in a 37 ℃ PBS solution for 24 h and then subjected to compression tests at room temperature (at a rate of 1 mm/min and a maximum compressive strain of 75%). The modulus of elasticity was determined as the slope within the linear region of the stress–strain curve for 5%–15% strain. All tests were carried out more than three times.

The tensile mechanical properties of the hydrogels were measured by a universal testing machine (INSTRON 3343, USA) using a 50 N pressure transducer. Test samples were prepared in a dumbbell shape (20 mm×2 mm×2 mm). Samples were incubated in 37 ℃ PBS solution for 24 h and then subjected to tensile testing at room temperature (at a rate of 1 mm/min and a maximum compressive strain of 75%) until fracture occurred. The modulus of elasticity was determined as the slope within the linear region of the stress–strain curve for 5%–15% strain. All tests were carried out more than three times.

2.8 Swelling ratio analysis

Samples were incubated in 37 ℃ PBS solution for 32 h. Samples were incubated in PBS solution at 5 min, 15 min, 30 min, 1 h, 2 h, 4 h, 8 h, 21 h, 27 h,

and 32 h, gently blotted dry, and weighed (W_S). The samples were then lyophilized and weighed to determine the dry weight (W_D). The swelling rate of the solubilized gel was calculated by

$$R_S = \frac{W_S - W_D}{W_D} \times 100\%. \quad (3)$$

2.9 Degradation study

Samples were placed in 500 μL of PBS and shaken at 37 ℃ at 140 r/min for three weeks to accelerate degradation. The PBS solution was renewed every 2–3 d to maintain a balanced concentration within the solution. At predetermined time points (12 h, 1 d, 3 d, 7 d, 11 d, 15 d, and 21 d), hydrogels were removed, rinsed twice with sterile deionized water, frozen, and weighed. The degradation rate of the gel was determined by

$$R_{DG} = \frac{W_0 - W_t}{W_0} \times 100\%, \quad (4)$$

where W_0 is the initial sample's dry weight and W_t is the dry weight after time t.

2.10 Cell viability

HUVECs were cultured in DMEM, supplemented with 10% FBS and 1% penicillin-streptomycin antibiotic solution at 37 ℃ and 5% CO_2. Cell proliferation was detected by the CCK-8 method. Briefly, cell proliferation on the samples was examined after incubation in electrospun membrane dip solution or in channel network hydrogel scaffolds.

In addition, the survival of cells after culturing on the surface of fibrous membrane and microchannel network hydrogel scaffolds of different formulations was tested by LIVE/DEAD assays. In general, HUVEC suspensions were inoculated on the surface of samples at a density of 1×10^4 cells/cm^2. After 7 d, the cells were assayed using calcein acetoxymethyl (AM) (green) and propidium iodide (PI) (red) and observed by the cell workstation.

2.11 Endothelial tube formation experiments on the surface and inside the scaffold

HUVECs were seeded on the surface of scaffolds to determine the feasibility of scaffolds for promoting endothelial cell tube formation. The prepared microchannel network scaffold was placed in each well of a 24-well plate. HUVECs at a density of 5×10^4 cells/well were seeded on the scaffold and cultured at 37 ℃ for 24 h. Endothelial tube formation images were taken using a cell workstation. The numbers of nodes/junctions and meshes were counted from 10 randomized low-power fields (LPFs) for each group.

To assess microchannel endothelialisation within the scaffold and to analyse cell morphology in comparison with the scaffold surface, HUVECs were stained with phalloidin and DAPI fluorescent dyes to visualise the nucleus and cytoskeleton when an intact endothelial monolayer was formed. HUVECs were seeded and then placed in a 5% CO_2 incubator at 37 ℃ for 30 min. Then, 300 μL of cell culture medium was added for incubation. After 3 d, the cells were fixed in 4% buffered paraformaldehyde and permeabilized with 0.2% Triton X-100 in PBS. Cellular F-actin filaments were stained with phalloidin at a final concentration of 200 units/mL, and nuclei were stained with DAPI solution. Ultimately, detailed high-resolution images were obtained using a confocal laser scanning microscope (CLSM).

2.12 Statistical analysis

All experiments were repeated independently three times. All quantitative data obtained from different assays were presented as the mean±standard error of mean. Comparisons between two groups were performed by independent t-test, whereas multiple comparisons were performed by one-way analysis of variance (ANOVA) with Tukey's post-hoc test using SPSS version 18.0. $P<0.05$ was considered statistically significant.

3 Results

3.1 Fabrication and characterization of sacrificial electrospun fibers

In this study, sacrificial template fibrous materials similar to the structure of natural capillary networks were constructed using the electrospinning technique. Through the optimisation of various influencing factors, micron-sized fibres of different diameters were obtained with an average diameter of more than 10 μm, allowing for better microchannel formation in hydrogels, which is of great significance for 3D cell culture studies.

The diameter of electrostatically spun fibers is positively related to the concentration of the solution.

First, to optimize the electrospinning parameters of PVA, different concentrations of PVA (10% and 15%) were dissolved in 1:2, 1:3, and 1:4 of deionized water: HFIP solutions. As the PVA concentration increased, the fiber diameter increased and gradually white fiber bundles could be seen to be adsorbed on the aluminum foil. Uniform, continuous fibers were observed under SEM (Fig. 1a) with good dispersion, and the average diameter of the samples was (14.64±8.98) μm (Fig. 1b).

Subsequently, the degradability of PVA in PBS solution was examined to allow for better elution at the expense of electrospun PVA fibers (Fig. 1c). The electrospun PVA fibers in PBS were degraded quickly in the first 10 min. The electrospun PVA fibers degraded by approximately 80% in 20 min. At the 60 min mark, the electrospun PVA fibers were almost completely degraded. The rapid degradation of electrospun PVA fibers can be regarded as a necessary condition for the formation of microporous channels within the GelMA hydrogel.

3.2 Fabrication of microchannel GelMA hydrogel scaffolds

Scheme 1 briefly describes the process and principles of preparing microchannel GelMA hydrogel bionic scaffolds. For GelMA hydrogels, hydrolysis from collagen can mimic the main components of the skin extracellular matrix, containing RGD sequences and matrix metalloproteinase MMPs, with better biocompatibility and lower immunogenicity (Eke et al., 2017). More importantly, the fidelity of microchannel formation within GelMA can be improved by increasing the concentration of GelMA hydrogels. As shown in Fig. 2a, characterization was carried out to verify that GelMA was synthesized from gelatine and MA. The absorption peaks at 3234 cm^{-1} were mainly N–H stretching vibrations corresponding to the presence of peptide bonds. The absorption peak at 1640 cm^{-1} was mainly the carbon–carbon double bond, exhibiting an increase in the intensity of GelMA, and representing the interaction between gelatine and methacrylic anhydride. The spectrum of GelMA showed an increase in the intensity of some peaks, particularly around 2352 cm^{-1}, which may be related to the MA grafted onto the gelatine. Figs. 2b and 2c show the NMR hydrogen spectra of gelatine and GelMA, respectively. Using the phenylalanine peak (7.2–7.5 ppm, 1 ppm=1×10^{-6}) as a standard in both different samples, a baseline correction was applied before obtaining the region of interest for the peak. The degree of methacrylate of gelatine was calculated from the proton NMR spectra of the gelatine aromatic amino acid residues at 7.4 ppm and the double bonds of the methacrylate group at 5.5 ppm and 5.7 ppm. The results of the proton NMR spectral characterization of this reaction indicated that the degree of methacrylate of gelatine was 77%.

The GelMA hydrogels were obtained by dissolving GelMA in a standard solution of LAP initiator and crosslinking it with UV. The prepared pure GelMA hydrogel scaffolds had a distinct morphology of pore-like structures, where the linkage between pore-like structures was reduced and became less numerous and the inter-pore wall thickness became smaller as the concentration of GelMA pre-crosslinking solution increased (Figs. 3a–3c). In addition, the microstructural properties and porosity of hydrogels are critical for cell and surrounding microenvironment interactions, so we investigated the effect of different concentrations on the porosity of engineered GelMA hydrogels (Fig. 3d). The results showed that the apparent pore size in the central region of the hydrogel decreased from (202.63±79.68) μm to (100.13±26.02) μm with increasing GelMA concentration. Thus, fibrous templates could

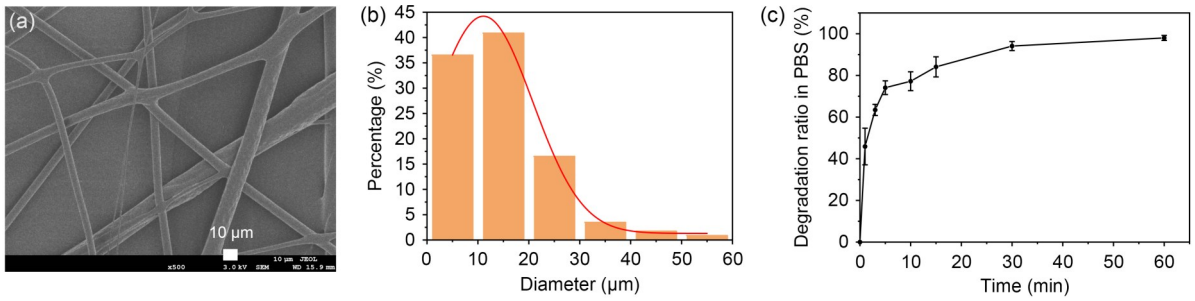

Fig. 1 Fabrication and characterization of PVA fibers: (a) SEM image of PVA fibers to study the surface of PVA fibers to mimic the capillary structure; (b) average diameter of PVA fibers; (c) degradation ratio of PVA fibers in PBS at room temperature

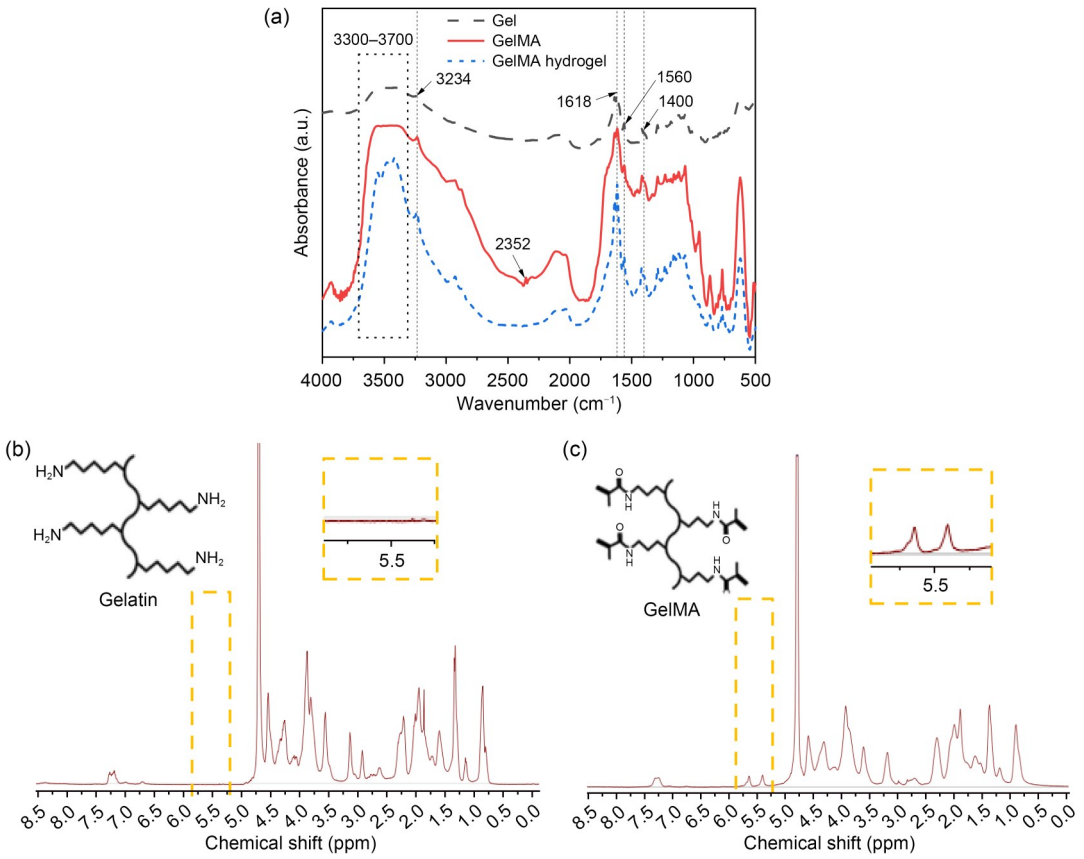

Fig. 2 Synthesis and characterization of GelMA hydrogels: FTIR spectra of gelatine, GelMA, and GelMA hydrogels (a); ^{1}H-NMR spectra of gelatin (b) and GelMA (c). ppm: parts per million (×10^{-6})

connect the pore-like structures, allowing the rapid migration and infiltration of cells. The PVA fibers were visible and well dispersed, allowing the fibers to be easily pulled apart. The fibers were filled with a pre-crosslinked GelMA hydrogel solution as described above, and then eluted with PBS in crosslinking curd hydrogels to obtain the original microchannel network scaffold (Fig. 3e). To observe the channel network formed after elution more clearly, we used anti-diffusion dye for perfusion. As shown in Fig. 3f, the channel network formed by perfusion can be observed clearly. Overall, the interconnected microchannel network in the GelMA hydrogel scaffold can provide structural advantages for nutrient transport and migration of cells in the scaffolds (Nichol et al., 2010; Wang et al., 2022; Zhang et al., 2022).

3.3 Mechanical properties

The mechanical properties were affected by the addition of microchannels within the GelMA hydrogel. As shown in Fig. 4, the tensile moduli of the three concentrations of pure GelMA hydrogels G-15, G-20, and G-25 were (65.82±7.98) kPa, (148.44±8.84) kPa, and (230.37±9.56) kPa, respectively. There was a significant increase in tensile mechanical properties with increasing GelMA concentration, which may be attributed to the increased crosslink density of GelMA hydrogels. The tensile moduli of the three concentrations of the microchannel network hydrogel scaffolds GC-15, GC-20, and GC-25 were (50.50±2.88) kPa, (89.92±9.14) kPa, and (106.97±2.69) kPa, respectively. Here, the formation of microchannels within the GelMA hydrogels by sacrificing the PVA fibers resulted in the disruption of their internal structure. However, the microchannel network hydrogel scaffold GC-20 was still suitable for the culture of endothelial cells (Zhao et al., 2016). In addition, the compression tests of pure GelMA hydrogels and microchannel network hydrogel scaffolds followed the same pattern (Figs. 4b and 4d). The moduli of compression for the three concentrations of pure GelMA hydrogels G-15, G-20, G-25, GC-15, GC-20, and GC-25 were (75.91±6.11) kPa,

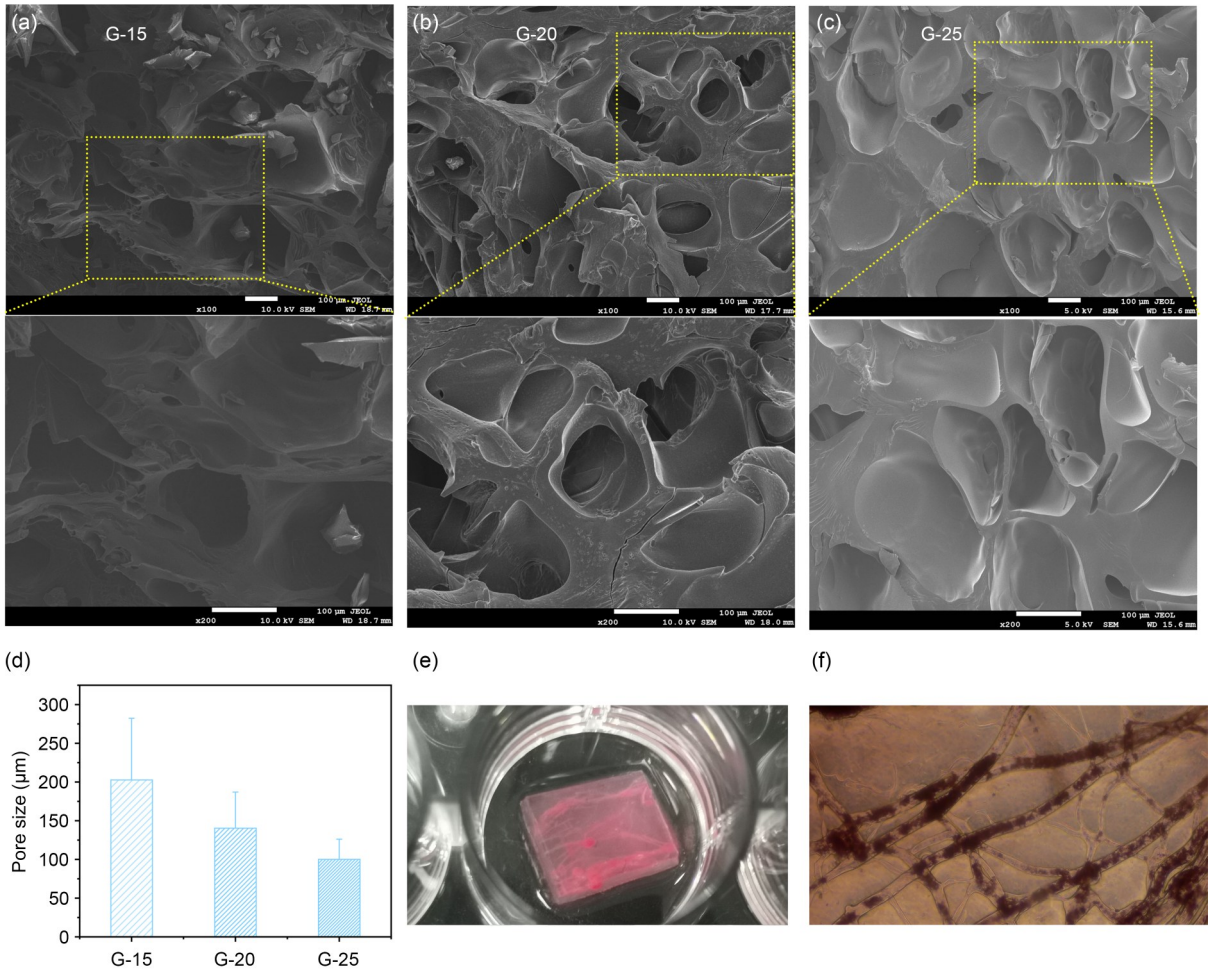

Fig. 3 Fabrication and characterization of microchannel GelMA hydrogels: (a–c) SEM images of GelMA hydrogels G15, G20, and G25; (d) quantification of GelMA hydrogel porosity from SEM images as a function of GelMA concentration; (e) image of microchannel network dye infusion; (f) microscopic image of microchannel network dye infusion

(120.64±8.10) kPa, (192.45±1.87) kPa, (9.81±5.74) kPa, (65.12±4.02) kPa, and (87.44±6.43) kPa, respectively. In comparison to the tensile test, the fragmentation of the scaffold was caused by the collapse of the microchannels within the GelMA hydrogel (Fig. 4b). As can be seen from the stress–strain curves, the scaffolds fragmented earlier as compression progressed and the stress-strain curves for the microchannel network scaffolds showed a similar increasing trend to the pure GelMA hydrogels. Overall, the mechanical properties of both pure GelMA hydrogel and microchannel network hydrogel scaffolds gained a significant enhancement with increasing concentration of GelMA hydrogel. Although the mechanical properties of both decreased with the addition of microchannel hydrogels, the elastic and compressive moduli (≈100 kPa) of both have been shown to favor the growth of HUVECs (Zhao et al., 2016).

3.4 Swelling

We further characterized the swelling rate of the hydrogel, which reflects its water absorption capacity and thus predicts its degradation rate. As shown in Fig. 5, it was found that the increase of the GelMA concentration from 15% to 25% resulted in a decrease of the swelling rate from 462% to 307% for pure GelMA hydrogels, and from 586% to 514% for microchannel network hydrogel scaffolds. The crosslink density of GelMA may not only affect the rate and amount of water penetration but was also thought to have influence on degradation. Interestingly, the addition of microchannels in GelMA hydrogels caused increases in swelling rates after they reached swelling equilibrium and the speed of degradation (Fig. S1 of the electronic supplementary materials). This may be due to the reduced

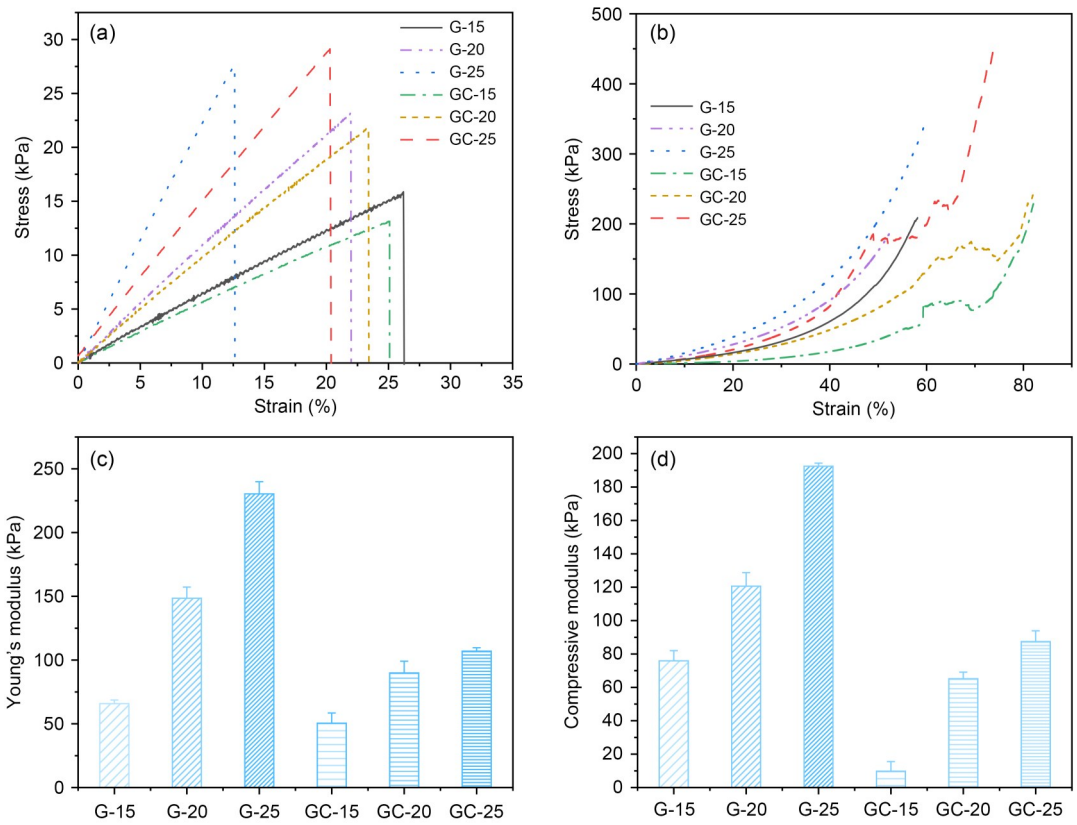

Fig. 4 Mechanical properties of pure GelMA and microchannel GelMA hydrogel scaffolds: stress–strain curves (G-15, G-20, G-25, GC-15, GC-20, and GC-25) of (a) tensile and (b) compression tests, and statistics of their (c) tensile modulus and (d) compressive modulus for pure GelMA hydrogel and microchanneled GelMA hydrogel scaffolds

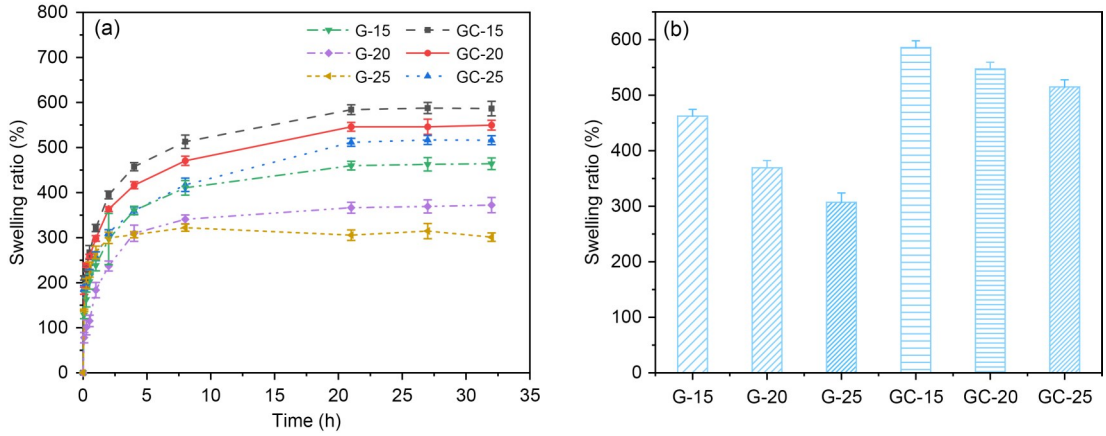

Fig. 5 Swelling properties of pure GelMA and microchannel network GelMA hydrogel scaffolds: (a) swelling curve; (b) swelling rate statistics

crosslink density and accelerate rate and amount of water penetration within GelMA hydrogels.

To determine the feasibility of microchannel hydrogel scaffolds for regenerative purposes, biodegradation profiles were assessed by using them in PBS solution. Here, pure GelMA hydrogels were used as control samples. The mass retention curves for three different concentrations of GelMA and microchannel GelMA hydrogels for 21 d are shown in Fig. S1. The results show that the degradation rate decreases with increasing GelMA concentration, with pure GelMA hydrogels being completely degraded in three weeks. Furthermore,

25% of the GelMA hydrogels were still present at more than 80% even after three weeks of incubation. The GelMA hydrogels incorporating microchannels degraded more rapidly than the pure GelMA hydrogels. Three of the microchannel GelMA hydrogels, GC-15, GC-20, and GC-25, had a mass retention of 0%, 32%, and 51% after 15 d. The microchannel hydrogel scaffold has an increased contact area with the solution and therefore it increases the degradation rate of the hybrid scaffold. Compared to previously developed collagen hydrogels (Helary et al., 2010, 2011, 2012), GelMA hydrogels are considered to be more suitable for long-term wound healing cases. They can remain in the wound bed for a long time, thus ensuring optimal healing while avoiding secondary infections.

The above results show that the mechanical and degradation properties of GelMA hydrogels can be modulated to a large extent by varying the GelMA concentration. The compression and elastic moduli can be adjusted from a few kilopascals to several hundred kilopascals, and degradation time can be retained for up to 51% for three weeks, demonstrating the broad performance of hydrogel as a tissue substitute in different body parts and different wound types.

3.5 Cell viability

In tissue engineering, ideal scaffolds are expected to promote cell migration, proliferation, and differentiation. The effect on cell viability is important due to the direct contact between cells and the scaffolds (Bae et al., 2011). In this study, biocompatible GelMA hydrogel with microchannels was prepared using PVA fibers as sacrificial material. HUVECs were cultured on hydrogel scaffolds to assess cytotoxicity and proliferative capacity using the CCK-8 method. As shown in Fig. S2, the extract of PVA fiber showed minimal cytotoxicity. Cell proliferation studies were performed on HUVECs using the CCK-8 method at four predetermined time points of 1, 3, 5, and 7 d (Fig. 6a). As shown in Fig. 6a, the optical density (OD) values of HUVECs on all the scaffolds increased with the culture time. On days 5 and 7, the OD values of HUVECs on GC-20 were higher than those of the other two. In addition, the potential toxicity of the developed hydrogel and its effect on cell behavior were systematically investigated using LIVE/DEAD assays, the results of which are shown in Fig. S3. There was no significant red fluorescence in the scaffolds. Therefore, GC-20 was chosen for subsequent experiments as it not only has good physical properties but also promotes cell proliferation. Furthermore, GelMA hydrogels can provide a 3D microenvironment similar to an extracellular matrix, which can be used to create complex, cell-responsive microtissues (Nichol et al., 2010; Chen et al., 2012; Lin et al., 2013).

3.6 Effects of scaffold surface and intra-scaffold microchannel on endothelial tube formation

The incorporation of microchannels within GelMA hydrogels is essential for the generation of tubular structures in HUVECs. Firstly, we observed the formation of endothelial rings on the scaffold surface by means of a cell workstation (Fig. 6b). The data showed that the numbers of endothelial nodes/junctions and meshes were significantly increased on the scaffold surface (2D culture) compared with the blank group (Figs. 6c and 6d). This result indicated the direct effect of GelMA hydrogels on angiogenesis in HUVECs. To further assess the changes in the cell morphology of HUVECs after ring formation on the GelMA hydrogel surface, we performed immunofluorescence staining of their nuclei and F-actin (Figs. S4 and 7a) and compared the cell morphology with that of the endothelial monomolecular layer cells within the microchannel (3D culture).

To demonstrate the feasibility of the use of fiber-forming microchannels in achieving artificial blood vessels, we introduced a standard vascular cell type, HUVECs, into the microchannels by direct extrusion perfusion and allowed it to achieve a confluent endothelial monolayer lining. We sacrificed the well-oriented template fibers embedded in the hydrogel matrix by lysis and, due to the excellent mechanical properties of this scaffold, repeated extrusion adequately elutes the PVA solution within the microchannel. To populate the microchannels with cells, the resulting microchannels were filled with a suspension of HUVECs by direct squeezing and the samples were placed statically in an incubator at 5% CO_2 and 37 °C for 30 min to support cells passing into the microchannel lumen. During the 3 d of static cell culture, the sidewalls of the microchannels within the hydrogel support adhesion and endothelial monolayer formation. Although dynamic culture can improve endothelialization outcomes, culturing cells under continuous flow conditions involves additional technical challenges, and we chose to use static cell culture. Cell proliferation was

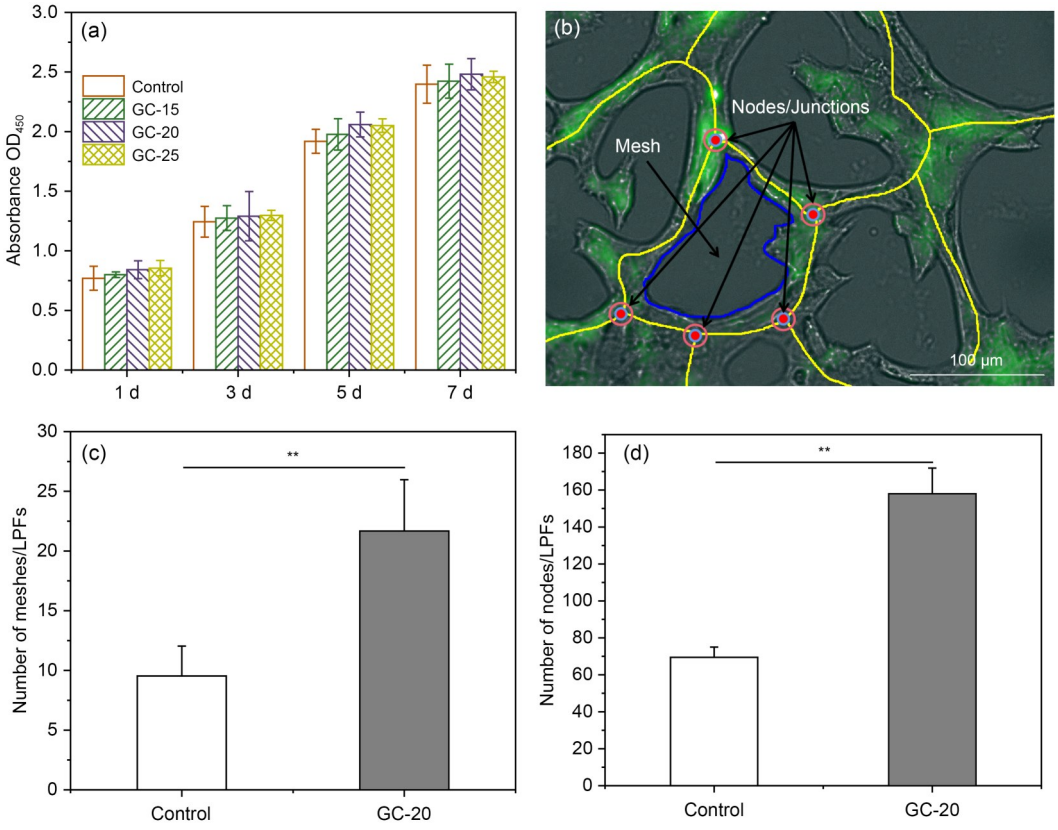

Fig. 6 Effect of scaffold surface on endothelial tube formation: (a) evaluation of cell viability of HUVECs on microchannel GelMA scaffolds; (b) localization of endothelial nodes/junctions (defined as junctions where at least three endothelial segments (walls) joined together) and mesh (defined as a complete loop of endothelial tubes surrounded by endothelial segments (walls)); (c and d) quantification of the numbers of meshes and nodes/junctions from each set of 10 random fluorescent images. Each bar represents the mean value of three independent experimental data. Data are presented as the mean±standard error of mean ($^{**}P$<0.01). OD_{450}: optical density at 450 nm

subsequently monitored by microscopy, and on day 3, monolayers of endothelial cells were attached to the lumen of the microchannel (Fig. 7b). We monitored HUVECs daily using bright field microscopy and, unlike other studies, no bioactive molecules promoting endothelial vascularisation were added, demonstrating that sacrificing fiber-patterned microchannels can support a functional and healthy endothelial monomolecular layer. Furthermore, the high activity of cells in the hydrogel, cell adhesion at the lateral end of the scaffold, the rapid proliferation, and vascularisation of endothelial cells in the spreading and patterned microchannels (Fig. 7c) demonstrated that the template fibers did not produce any significant toxic by-products.

To investigate the effect of the local 3D microchannel structure on the behavior and growth state of HUVECs, the growth morphology of HUVECs on the surface of the scaffold (2D) and within the lumen of the microchannel (3D) was assessed. Obviously, the morphology of HUVECs differs in different microenvironments. In the 2D matrix, the HUVECs were more densely distributed and showed a stacked state, with a tendency to develop toward a 3D structure (Fig. 7a). Within the 3D scaffold, the cells show a typical homogeneous endothelial monomolecular layer (Fig. 7c, magnified image).

Next, we measured the morphology of the nuclei e.g., long-axis length, area, and aspect ratio (Fig. S5). The results showed that the 3D matrix significantly enhanced the spreading area and length of the nucleus compared to the 2D matrix. This suggests that the cells spread well within the lumen by deforming to fit the microchannel structure through the cellular perception of the external microenvironment ((193.50±38.38) μm^2, (18.09±2.97) μm in the 3D matrix, and (128.62±26.94) μm^2, (15.39±1.84) μm on the 2D matrix (Figs. 8a and 8c)). Furthermore, the average nucleus aspect ratio of HUVECs on the 2D matrix was significantly higher

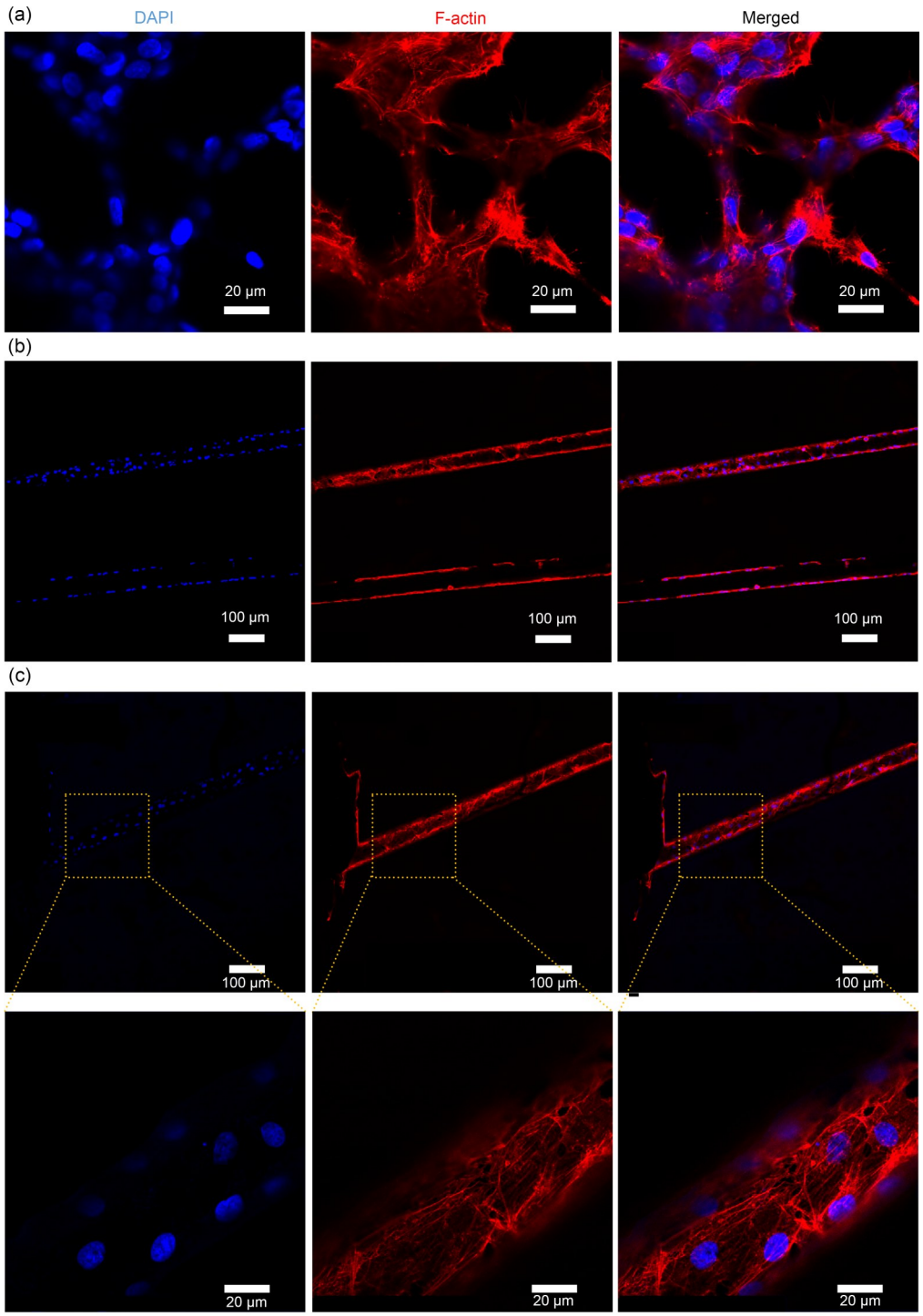

Fig. 7 Effects of intra-scaffold microchannel networks on endothelial tube formation: CLSM images after immunofluorescence staining of the nucleus (blue) and F-actin (red) of the endothelial monomolecular layer on the GC-20 scaffold surface (a); CLSM images on the lumen of the microchannel in the GC-20 scaffold near the central part of the scaffold (b) and near the edge of the scaffold (c) (magnification of 10×, 40×, and 63×, respectively). References to color refer to the online version of this figure

than for those in the 3D matrix (1.71 and 1.43, respectively) (Fig. 8b). Thus, in summary, HUVECs in the 3D matrix showed a typical cobblestone-like endothelium structure, whereas cells on the 2D matrix showed a longer cell morphology due to the formation of the applicable ring-like structure. In addition, we measured the

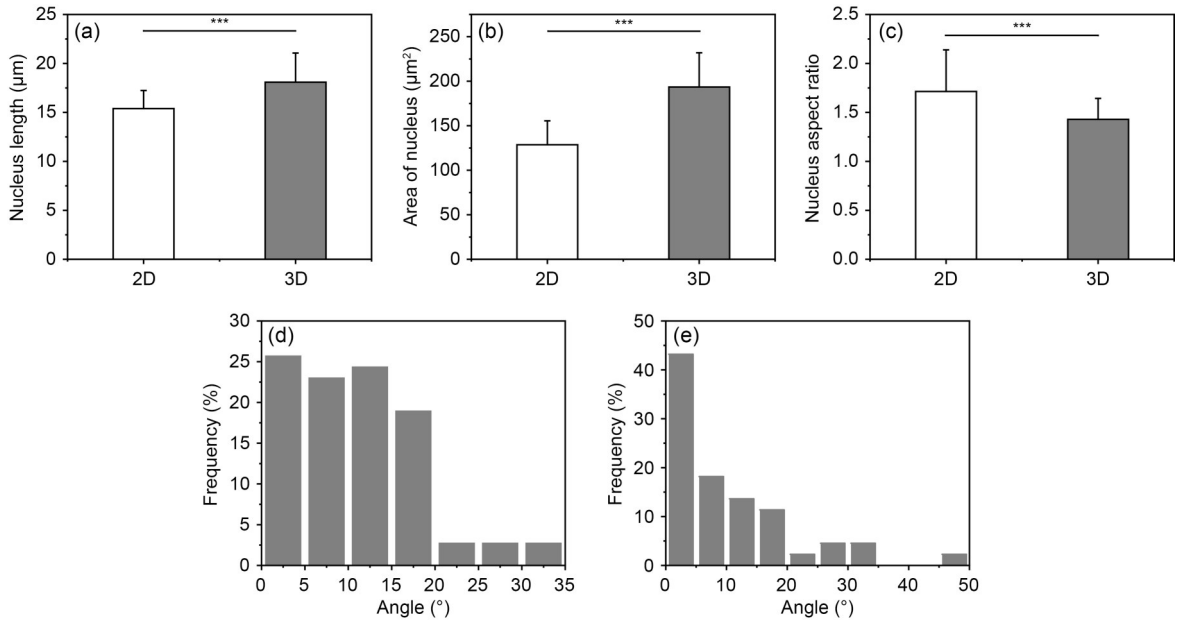

Fig. 8 Quantitative comparison of endothelial cell nucleus length (a), area (b), aspect ratio (c), and pinch angle under 2D (d) and 3D (e) matrix conditions. Data are expressed as the mean±standard error of mean, $n \geqslant 3$ ($^{***}P<0.001$)

angle of the long axis of the nucleus, for the 2D and the 3D matrices, to the tangent of the cell ring and the main axis of the microchannel, respectively. As shown in Figs. 8d and 8e, the majority of cells (>80%) favored either the cell ring or the main axis of the microchannel. In conclusion, the 3D ECM microenvironment provided by a high concentration of GelMA hydrogel scaffolds containing microchannels can influence the cell behavior and morphology of HUVECs through contact guidance, thereby promoting a homogeneous endothelial monomolecular layer.

4 Discussion

This study presents a method for the preparation of 3D hydrogels embedded within a mimetic branching microvessel that mimics the native tissue structure of ECM. By electrospinning in the microchannel-containing mimetic tissue structure, the scaffold with microporous channels ensures the permeability of the final structure to achieve a high-resolution scaffold structure at the micrometer scale to facilitate the formation of endothelial cell monomolecular layers by HUVECs.

By optimizing the dispersion of electrospun fibers, the original structure of the sacrificial fiber template was adapted to form naturally branching and interconnected microchannel networks in hydrogels. The need to form complex and interconnected networks to simulate vascular systems has led to the development of various sacrificial template methods over the last few years. However, limitations in the resolution of the process and spatial considerations in the fabrication of 3D structures were two challenging factors for the realization of microvascular systems with this approach. The significant advantage of the fiber template designed in this study is that it breaks through in the tunability of electrospinning in the manufacture of micron-scale production and can be used to create predictable and defined micro-scale network architectures that mimic native capillaries, depending on the size requirements.

The production of fibrous templates by electrospinning is particularly interesting as achieving high resolution is a key challenge for other channel creation methods. The fabrication of microchannels that mimic capillary networks is essential to ensure the uniform distribution of nutrients and oxygen in larger hydrogel structures and, so far, biocompatible templates for microchannels have mainly used heat-responsive sacrificial structures (Kolesky et al., 2014, 2016; Tsai et al., 2020; Davoodi et al., 2022) or water-soluble carbohydrate-based structures (Miller et al., 2012; Gryka et al., 2019). Daly et al. (2018) used sacrificial pluronic inks in mesenchymal stem cell (MSC)-loaded GelMA hydrogels to 3D print interconnected microchannel networks. Zhou et al. (2022) developed a

catechol-functionalized ink system to produce tough and elastic scaffolds with built-in microchannels that mimic vascular structures; these approaches can achieve significant levels of geometric complexity for achieving interconnected channels. However, key bottlenecks include some design aspects such as the circularity of the microchannels and the creation of overhanging branching sacrificial structures, and the scale aspect of the sacrificial template. Also, the microchannel networks prepared by this method have difficulty in simulating the complexity of microvascular structures within native tissues.

As an alternative to existing sacrificial materials, we have used water-soluble PVA because of its inherent biocompatibility and its unique electrostatically induced plasticity. The low alcohol solubility of PVA allows for rapid dissolution at room temperature. As a result, pre-crosslinked GelMA solutions allow rapid encapsulation of low alcohol-degradable PVA fibrous structural fibers without loss of scaffold integrity, avoiding the fusion of adjacent fibers during the gelation of the hydrogel matrix. GelMA hydrogels were induced to form a natural tissue structure mimicking a capillary-containing network, and the PVA solution within the channel network was eluted by repeated extrusion under room temperature conditions. Perfusion of engineered microvasculature was established in the hydrogel, as evidenced by the presence of diffusion-resistant dye within the microchannel network alone, and the GelMA hydrogel could be demonstrated to have good tunability and resolution of stereoscopic micropatterning.

The mechanical properties of hydrogel scaffolds have different effects on endothelial cell behaviour and microvascular networks (Yamamura et al., 2007). For example, microvascular networks invade more deeply in rigid gels than in flexible gels. Cells in flexible gels invade the gel independently, forming networks that are predominantly distributed at a depth of <30 μm. In contrast, in rigid gels, the balance shifts towards morphogenetic properties at the expense of migratory activity. In order to control the 3D conformation of the network, a balance between migratory activity and morphogenetic properties is important. In the work presented here, we have demonstrated that the stiffness of 20% GelMA hydrogels affects the proliferation of HUVECs and the formation of endothelial monomolecular layers within the channel. Increasing the stiffness of the scaffold by increasing the concentration of GelMA hydrogel ensures various physical properties of the hydrogel as a scaffold. Secondly, endothelial cells may require more ECM remodelling active material to penetrate the rigid gel, which may result in reduced migration activity. Thus, the incorporation of microchannels within high concentrations of GelMA hydrogels not only increases cell permeation and nutrient diffusion but the ECs in the 3D matrix promote morphogenesis, and the suitably reduced mechanical properties of GelMA hydrogels may be more conducive to the formation of EC monolayers.

The lack of a vascular network may limit oxygen diffusion in thicker 3D tissue models and lead to cell death due to hypoxia. Thus, vascularisation remains a key challenge for engineered tissues and their successful translation into clinical tissue regeneration. In this study, we used HUVECs to successfully form an endothelial monomolecular layer in a 3D tissue model containing a microchannel network. Microchannel endothelialization within hydrogels was performed by short-term static cell seeding, starting with squeeze perfusion resting for 30 min to allow initial cell attachment. After 3–4 d of culture using this method, HUVECs spontaneously arranged into an endothelial monolayer lined with the interior of the microchannel, pointing to the potential of using our platform to promote vascularisation to investigate the effect of channel size on neovascularisation and revascularization. In line with the results of Enrico et al. (2022), this 3D channel was confirmed to form artificial microvessels through endothelial cell culture and cell media perfusion. F-actin/DAPI staining showed that the nuclei of HUVECs were evenly distributed within the lumen of the microchannel; microfilaments were clearly visible and spread in an elongated structure within the channel lumen, and cells were more tightly connected (Fig. 7b). Consistent with other studies (Atia et al., 2018), under static conditions, the luminal HUVECs formed an elongated shape due to the low number of cells, suggesting that pro-angiogenic conditions trigger higher cell viability and thus the formation of an endothelial monomolecular layer. At the same time, this further confirms the continuity and patency of pore formation within the GelMA hydrogel and the feasibility and robustness of hydrogel mechanical properties for microvessel formation.

Furthermore, the integrity and effectiveness of engineered vascular networks are key challenges in regenerative medicine. Vascular heterogeneity does not

allow ECs from different adult tissues or pluripotent stem cells to mimic the specific microvasculature of the corresponding tissues. In recent work, Song et al. (2022) established a method to dilate tubular microvessels with ECs and pericytes from the same adult tissue on 2D rigid substrates for investigating the mechanisms of EC-pericyte interactions in tissue regeneration and disease. The hydrogel 3D scaffold platform containing the microchannel network proposed in this study can be further used for the study of EC-pericyte interaction mechanisms, which is beneficial for the development of personalized microvascular engineering for precision medicine. In addition, Gao et al. (2022) investigated the generation of microvessels by human pluripotent stem cells (iMVs) and validated the potential of iMVs for rapid angiogenesis and tissue repair. Therefore, in the future, it is crucial that we should validate the hydrogel scaffold platform in combination with other rapidly vascularised cells or units for validation applications and also undertake further animal studies to assess the safety and efficacy of this model before it is translated into the clinic.

In summary, this study presents a high-precision microfabrication strategy suitable for the fabrication of tissue models simulating endocapillary networks, which will enable their translation into clinically relevant implants. Furthermore, this approach is expected to advance the field of tissue engineering and regenerative medicine by opening up new opportunities for exploring the effects of well-controlled 3D microgeometry on cell behavior.

5 Conclusions

This study introduced an integrative and straightforward approach combining the sacrificial template method with electrospinning to fabricate microchannel network biomimetic hydrogel scaffolds that mimic the native structure and microenvironment of the ECM. Fibers were prepared by electrospinning technology. Moreover, GelMA hydrogels were induced to form mimetic natural tissue structures mimicking capillary networks by extrusion elution. The results showed that GelMA hydrogels have an excellent impact on the viability, distribution, and alignment of HUVECs.

The design for microvascular networks, the flexibility of the hydrogel matrix properties, and the rapid functional endothelialization allow us to address some of the limitations of current methods for creating microvascular structures. Therefore, the present findings provide new insight into 3D tissue hydrogel models as a widely applicable alternative platform for generating vascularised tissue models.

Acknowledgments

This work is supported by the National Natural Science Foundation of China (No. 31870934) and the Natural Science Foundation for Young Scientists of Shanxi Province (No. 202103021223100), China.

Author contributions

Haoyu SUN, Yang LIU, Meiwen AN, Meiling WEN, and Li WANG designed the research. Haoyu SUN, Haiyang MA, Tian HOU, Wenjie TANG, and Qing YU processed the corresponding data. Haoyu SUN wrote the first draft of the manuscript. Meiling WEN helped to organize the manuscript. Meiwen AN revised and edited the final version.

Conflict of interest

Haoyu SUN, Haiyang MA, Li WANG, Yang LIU, Tian HOU, Wenjie TANG, Qing YU, Meiwen AN, and Meiling WEN declare that they have no conflict of interest.

References

Atia L, Bi DP, Sharma Y, et al., 2018. Geometric constraints during epithelial jamming. *Nature Physics*, 14(6):613-620. https://doi.org/10.1038/s41567-018-0089-9

Aubin H, Nichol JW, Hutson CB, et al., 2010. Directed 3D cell alignment and elongation in microengineered hydrogels. *Biomaterials*, 31(27):6941-6951. https://doi.org/10.1016/j.biomaterials.2010.05.056

Bacakova L, Pajorova J, Bacakova M, et al., 2019. Versatile application of nanocellulose: from industry to skin tissue engineering and wound healing. *Nanomaterials*, 9(2):164. https://doi.org/10.3390/nano9020164

Bae H, Ahari AF, Shin H, et al., 2011. Cell-laden microengineered pullulan methacrylate hydrogels promote cell proliferation and 3D cluster formation. *Soft Matter*, 7(5): 1903-1911. https://doi.org/10.1039/C0SM00697A

Bertassoni LE, Cecconi M, Manoharan V, et al., 2014. Hydrogel bioprinted microchannel networks for vascularization of tissue engineering constructs. *Lab on a Chip*, 14(13):2202-2211. https://doi.org/10.1039/c4lc00030g

Boakye MAD, Rijal NP, Adhikari U, et al., 2015. Fabrication and characterization of electrospun PCL-MgO-keratin-based composite nanofibers for biomedical applications. *Materials*, 8(7):4080-4095. https://doi.org/10.3390/ma8074080

Buchwald P, 2009. FEM-based oxygen consumption and cell

viability models for avascular pancreatic islets. *Theoretical Biology and Medical Modelling*, 6:5. https://doi.org/10.1186/1742-4682-6-5

Bupphathong S, Quiroz C, Huang W, et al., 2022. Gelatin methacrylate hydrogel for tissue engineering applications–a review on material modifications. *Pharmaceuticals*, 15(2): 171. https://doi.org/10.3390/ph15020171

Chamorro CI, Zeiai S, Reinfeldt Engberg G, et al., 2016. Minced tissue in compressed collagen: a cell-containing biotransplant for single-staged reconstructive repair. *Journal of Visualized Experiments*, 108:53061. https://doi.org/10.3791/53061

Chang WG, Niklason LE, 2017. A short discourse on vascular tissue engineering. *NPJ Regenerative Medicine*, 2:7. https://doi.org/10.1038/s41536-017-0011-6

Chen YC, Lin RZ, Qi H, et al., 2012. Functional human vascular network generated in photocrosslinkable gelatin methacrylate hydrogels. *Advanced Functional Materials*, 22(10): 2027-2039. https://doi.org/10.1002/adfm.201101662

Cicha I, Detsch R, Singh R, et al., 2017. Biofabrication of vessel grafts based on natural hydrogels. *Current Opinion in Biomedical Engineering*, 2:83-89. https://doi.org/10.1016/j.cobme.2017.05.003

Daly AC, Pitacco P, Nulty J, et al., 2018. 3D printed microchannel networks to direct vascularisation during endochondral bone repair. *Biomaterials*, 162:34-46. https://doi.org/10.1016/j.biomaterials.2018.01.057

Davoodi E, Montazerian H, Zhianmanesh M, et al., 2022. Template-enabled biofabrication of thick 3D tissues with patterned perfusable macrochannels. *Advanced Healthcare Materials*, 11(7):2102123. https://doi.org/10.1002/adhm.202102123

Dogan E, Bhusal A, Cecen B, et al., 2020. 3D printing metamaterials towards tissue engineering. *Applied Materials Today*, 20:100752. https://doi.org/10.1016/j.apmt.2020.100752

Duval K, Grover H, Han LH, et al., 2017. Modeling physiological events in 2D vs. 3D cell culture. *Physiology*, 32(4): 266-277. https://doi.org/10.1152/physiol.00036.2016

Edwards A, Jarvis D, Hopkins T, et al., 2015. Poly(ε-caprolactone)/keratin-based composite nanofibers for biomedical applications. *Journal of Biomedical Materials Research Part B: Applied Biomaterials*, 103(1):21-30. https://doi.org/10.1002/jbm.b.33172

Eke G, Mangir N, Hasirci N, et al., 2017. Development of a UV crosslinked biodegradable hydrogel containing adipose derived stem cells to promote vascularization for skin wounds and tissue engineering. *Biomaterials*, 129:188-198. https://doi.org/10.1016/j.biomaterials.2017.03.021

Enrico A, Voulgaris D, Östmans R, et al., 2022. 3D microvascularized tissue models by laser-based cavitation molding of collagen. *Advanced Materials*, 34(11):2109823. https://doi.org/10.1002/adma.202109823

Gao X, Ma SX, Xing XT, et al., 2022. Microvessels derived from hiPSCs are a novel source for angiogenesis and tissue regeneration. *Journal of Tissue Engineering*, 13:1-21. https://doi.org/10.1177/20417314221143240

Groebe K, Mueller-Klieser W, 1991. Distributions of oxygen, nutrient, and metabolic waste concentrations in multicellular spheroids and their dependence on spheroid parameters. *European Biophysics Journal*, 19(4):169-181. https://doi.org/10.1007/BF00196343

Gryka MC, Comi TJ, Forsyth RA, et al., 2019. Controlled dissolution of freeform 3D printed carbohydrate glass scaffolds in hydrogels using a hydrophobic spray coating. *Additive Manufacturing*, 26:193-201. https://doi.org/10.1016/j.addma.2018.12.014

Helary C, Bataille I, Abed A, et al., 2010. Concentrated collagen hydrogels as dermal substitutes. *Biomaterials*, 31(3): 481-490. https://doi.org/10.1016/j.biomaterials.2009.09.073

Helary C, Abed A, Mosser G, et al., 2011. Synthesis and in vivo integration of improved concentrated collagen hydrogels. *Journal of Tissue Engineering and Regenerative Medicine*, 5(3):248-252. https://doi.org/10.1002/term.326

Helary C, Zarka M, Giraud-Guille MM, 2012. Fibroblasts within concentrated collagen hydrogels favour chronic skin wound healing. *Journal of Tissue Engineering and Regenerative Medicine*, 6(3):225-237. https://doi.org/10.1002/term.420

Hinton TJ, Jallerat Q, Palchesko RN, et al., 2015. Three-dimensional printing of complex biological structures by freeform reversible embedding of suspended hydrogels. *Science Advances*, 1(9):e1500758. https://doi.org/10.1126/sciadv.1500758

Hu KK, Shi H, Zhu J, et al., 2010. Compressed collagen gel as the scaffold for skin engineering. *Biomedical Microdevices*, 12(4):627-635. https://doi.org/10.1007/s10544-010-9415-4

Kenar H, Ozdogan CY, Dumlu C, et al., 2019. Microfibrous scaffolds from poly($_L$-lactide-*co*-ε-caprolactone) blended with xeno-free collagen/hyaluronic acid for improvement of vascularization in tissue engineering applications. *Materials Science and Engineering: C*, 97:31-44. https://doi.org/10.1016/j.msec.2018.12.011

Kim MS, Kim G, 2014. Three-dimensional electrospun polycaprolactone (PCL)/alginate hybrid composite scaffolds. *Carbohydrate Polymers*, 114:213-221. https://doi.org/10.1016/j.carbpol.2014.08.008

Kolesky DB, Truby RL, Gladman AS, et al., 2014. 3D bioprinting of vascularized, heterogeneous cell-laden tissue constructs. *Advanced Materials*, 26(19):3124-3130. https://doi.org/10.1002/adma.201305506

Kolesky DB, Homan KA, Skylar-Scott MA, et al., 2016. Three-dimensional bioprinting of thick vascularized tissues. *Proceedings of the National Academy of Sciences of the United States of America*, 113(12):3179-3184. https://doi.org/10.1073/pnas.1521342113

Kumar M, Sharma V, 2021. Additive manufacturing techniques for the fabrication of tissue engineering scaffolds: a review. *Rapid Prototyping Journal*, 27(6):1230-1272. https://doi.org/10.1108/rpj-01-2021-0011

Kurakula M, Koteswara Rao GSN, 2020. Moving polyvinyl pyrrolidone electrospun nanofibers and bioprinted scaffolds toward multidisciplinary biomedical applications. *European Polymer Journal*, 136:109919. https://doi.org/10.1016/j.eurpolymj.2020.109919

Li Y, Wang J, Wang Y, et al., 2021. Advanced electrospun hydrogel fibers for wound healing. *Composites Part B: Engineering*, 223:109101. https://doi.org/10.1016/j.compositesb.2021.109101

Liaw CY, Guvendiren M, 2017. Current and emerging applications of 3D printing in medicine. *Biofabrication*, 9(2): 024102. https://doi.org/10.1088/1758-5090/aa7279

Lin RZ, Chen YC, Moreno-Luna R, et al., 2013. Transdermal regulation of vascular network bioengineering using a photopolymerizable methacrylated gelatin hydrogel. *Biomaterials*, 34(28):6785-6796. https://doi.org/10.1016/j.biomaterials.2013.05.060

Lovett ML, Nieland TJF, Dingle YTL, et al., 2020. Innovations in 3D tissue models of human brain physiology and diseases. *Advanced Functional Materials*, 30(44):1909146. https://doi.org/10.1002/adfm.201909146

Miller JS, Stevens KR, Yang MT, et al., 2012. Rapid casting of patterned vascular networks for perfusable engineered three-dimensional tissues. *Nature Materials*, 11(9):768-774. https://doi.org/10.1038/NMAT3357

Mota C, Puppi D, Chiellini F, et al., 2015. Additive manufacturing techniques for the production of tissue engineering constructs. *Journal of Tissue Engineering and Regenerative Medicine*, 9(3):174-190. https://doi.org/10.1002/term.1635

Moulisová V, Gonzalez-García C, Cantini M, et al., 2017. Engineered microenvironments for synergistic VEGF-integrin signalling during vascularization. *Biomaterials*, 126:61-74. https://doi.org/10.1016/j.biomaterials.2017.02.024

Nazarnezhad S, Baino F, Kim HW, et al., 2020. Electrospun nanofibers for improved angiogenesis: promises for tissue engineering applications. *Nanomaterials*, 10(8):1609. https://doi.org/10.3390/nano10081609

Nichol JW, Koshy ST, Bae H, et al., 2010. Cell-laden microengineered gelatin methacrylate hydrogels. *Biomaterials*, 31(21):5536-5544. https://doi.org/10.1016/j.biomaterials.2010.03.064

Pien N, Pezzoli D, van Hoorick J, et al., 2021. Development of photo-crosslinkable collagen hydrogel building blocks for vascular tissue engineering applications: a superior alternative to methacrylated gelatin? *Materials Science and Engineering: C*, 130:112460. https://doi.org/10.1016/j.msec.2021.112460

Rademakers T, Horvath JM, van Blitterswijk CA, et al., 2019. Oxygen and nutrient delivery in tissue engineering: approaches to graft vascularization. *Journal of Tissue Engineering and Regenerative Medicine*, 13(10):1815-1829. https://doi.org/10.1002/term.2932

Rnjak-Kovacina J, Wray LS, Golinski JM, et al., 2014. Arrayed hollow channels in silk-based scaffolds provide functional outcomes for engineering critically sized tissue constructs. *Advanced Functional Materials*, 24(15):2188-2196. https://doi.org/10.1002/adfm.201302901

Roh TT, Chen Y, Paul HT, et al., 2019. 3D bioengineered tissue model of the large intestine to study inflammatory bowel disease. *Biomaterials*, 225:119517. https://doi.org/10.1016/j.biomaterials.2019.119517

Rouwkema J, Rivron NC, van Blitterswijk CA, 2008. Vascularization in tissue engineering. *Trends in Biotechnology*, 26(8):434-441. https://doi.org/10.1016/j.tibtech.2008.04.009

Ryma M, Genç H, Nadernezhad A, et al., 2022. A print-and-fuse strategy for sacrificial filaments enables biomimetically structured perfusable microvascular networks with functional endothelium inside 3D hydrogels. *Advanced Materials*, 34(28):2200653. https://doi.org/10.1002/adma.202200653

Shiwarski DJ, Hudson AR, Tashman JW, et al., 2021. Emergence of fresh 3D printing as a platform for advanced tissue biofabrication. *APL Bioengineering*, 5(1):010904. https://doi.org/10.1063/5.0032777

Song XY, Yu YL, Leng Y, et al., 2022. Expanding tubular microvessels on stiff substrates with endothelial cells and pericytes from the same adult tissue. *Journal of Tissue Engineering*, 13:1-17. https://doi.org/10.1177/20417314221125310

Therriault D, White SR, Lewis JA, 2003. Chaotic mixing in three-dimensional microvascular networks fabricated by direct-write assembly. *Nature Materials*, 2(4):265-271. https://doi.org/10.1038/nmat863

Toriello M, Afsari M, Shon HK, et al., 2020. Progress on the fabrication and application of electrospun nanofiber composites. *Membranes*, 10(9):204. https://doi.org/10.3390/membranes10090204

Tsai YL, Theato P, Huang CF, et al., 2020. A 3D-printable, glucose-sensitive and thermoresponsive hydrogel as sacrificial materials for constructs with vascular-like channels. *Applied Materials Today*, 20:100778. https://doi.org/10.1016/j.apmt.2020.100778

Türker E, Yildiz ÜH, Arslan Yildiz A, 2019. Biomimetic hybrid scaffold consisting of co-electrospun collagen and PLLCL for 3D cell culture. *International Journal of Biological Macromolecules*, 139:1054-1062. https://doi.org/10.1016/j.ijbiomac.2019.08.082

Uppuluri VNVA, Thukani Sathanantham S, Bhimavarapu SK, et al., 2022. Polymeric hydrogel scaffolds: skin tissue engineering and regeneration. *Advanced Pharmaceutical Bulletin*, 12(3):437-448. https://doi.org/10.34172/apb.2022.069

van den Bulcke AI, Bogdanov B, de Rooze N, et al., 2000. Structural and rheological properties of methacrylamide modified gelatin hydrogels. *Biomacromolecules*, 1(1):31-38. https://doi.org/10.1021/bm990017d

Wan XZ, Liu PC, Jin XX, et al., 2018. Electrospun PCL/keratin/auNPs mats with the catalytic generation of nitric oxide for potential of vascular tissue engineering. *Journal of Biomedical Materials Research Part A*, 106(12):3239-3247. https://doi.org/10.1002/jbm.a.36521

Wang Y, Kankala RK, Ou CW, et al., 2022. Advances in hydrogel-based vascularized tissues for tissue repair and

drug screening. *Bioactive Materials*, 9:198-220. https://doi.org/10.1016/j.bioactmat.2021.07.005

Wittmer CR, Hu X, Gauthier PC, et al., 2011. Production, structure and in vitro degradation of electrospun honeybee silk nanofibers. *Acta Biomaterialia*, 7(10):3789-3795. https://doi.org/10.1016/j.actbio.2011.06.001

Xia P, Luo YX, 2022. Vascularization in tissue engineering: the architecture cues of pores in scaffolds. *Journal of Biomedical Materials Research Part B: Applied Biomaterials*, 110(5):1206-1214. https://doi.org/10.1002/jbm.b.34979

Xiao SN, Zhao TF, Wang JK, et al., 2019. Gelatin methacrylate (GelMA)-based hydrogels for cell transplantation: an effective strategy for tissue engineering. *Stem Cell Reviews and Reports*, 15(5):664-679. https://doi.org/10.1007/s12015-019-09893-4

Xu F, Dawson C, Lamb M, et al., 2022. Hydrogels for tissue engineering: addressing key design needs toward clinical translation. *Frontiers in Bioengineering and Biotechnology*, 10:849831. https://doi.org/10.3389/fbioe.2022.849831

Yamamura N, Sudo R, Ikeda M, et al., 2007. Effects of the mechanical properties of collagen gel on the in vitro formation of microvessel networks by endothelial cells. *Tissue Engineering*, 13(7):1443-1453. https://doi.org/10.1089/ten.2006.0333

Zhang YY, Chen H, Li JS, 2022. Recent advances on gelatin methacrylate hydrogels with controlled microstructures for tissue engineering. *International Journal of Biological Macromolecules*, 221:91-107. https://doi.org/10.1016/j.ijbiomac.2022.08.171

Zhao DK, Xu HQ, Yin J, et al., 2022. Inkjet 3D bioprinting for tissue engineering and pharmaceutics. *Journal of Zhejiang University-SCIENCE A (Applied Physics & Engineering)*, 23(12):955-973. https://doi.org/10.1631/2023.A2200569

Zhao X, Lang Q, Yildirimer L, et al., 2016. Photocrosslinkable gelatin hydrogel for epidermal tissue engineering. *Advanced Healthcare Materials*, 5(1):108-118. https://doi.org/10.1002/adhm.201500005

Zhou Y, Fan YC, Chen Z, et al., 2022. Catechol functionalized ink system and thrombin-free fibrin gel for fabricating cellular constructs with mechanical support and inner micro channels. *Biofabrication*, 14(1):015004. https://doi.org/10.1088/1758-5090/ac2ef8

Zia AW, Liu R, Wu X, 2022. Structural design and mechanical performance of composite vascular grafts. *Bio-Design and Manufacturing*, 5(4):757-785. https://doi.org/10.1007/s42242-022-00201-7

Zohar B, Blinder Y, Mooney DJ, et al., 2018. Flow-induced vascular network formation and maturation in three-dimensional engineered tissue. *ACS Biomaterials Science & Engineering*, 4(4):1265-1271.

Electronic supplementary materials

Figs. S1–S5